This manuscript is a preprint for EarthArXiv and has been submitted to *Advances in Water Resources* for review.

We welcome helpful feedback.

Authors: Anupal Baruah[a] , Gilbert Hinge[b] , Omar Wani[c*]

a University of Alabama, Department of Geography and Environment, Tuscaloosa, 35401, AL, United States of America

b National Institute of Technology Durgapur, Department of Civil Engineering, Durgapur, 713209, West Bengal, India

c New York University, Tandon School of Engineering, Brooklyn, 11201, NY, United States of America

* Correspondence: omarwani@nyu.edu

Graphical Abstract

Flooding, nonlinear dynamics and Jensen's inequality: Analyzing the damping and amplification of inundation extent with river discharge nonstationarity

Anupal Baruah[a], Gilbert Hinge[b], Omar Wani[c*]

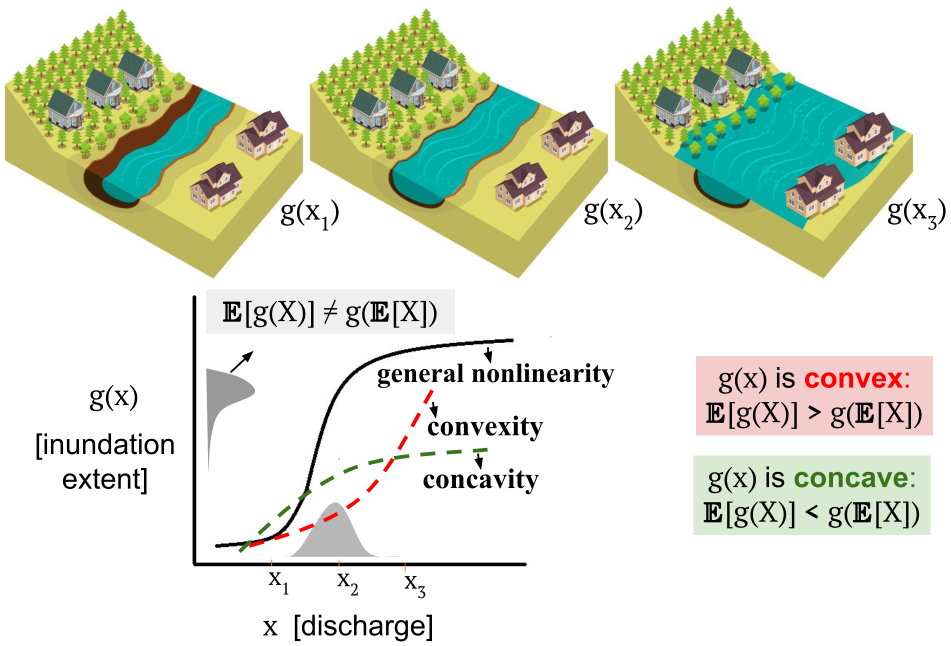

Highlights

Flooding, nonlinear dynamics and Jensen's inequality: Analyzing the damping and amplification of inundation extent with river discharge nonstationarity

Anupal Baruah[a], Gilbert Hinge[b], Omar Wani[c*]

- The relationship between inundation extent and river discharge is nonlinear.
- We introduce Jensen's Inundation Factor (JIF) to characterize this nonlinearity.
- We discuss the damping and amplification in inundation with shifts in discharge.
- JIF provides insights on critical thresholds related to flood inundation risk.

Flooding, nonlinear dynamics and Jensen's inequality: Analyzing the damping and amplification of inundation extent with river discharge nonstationarity

Anupal Baruah[a], Gilbert Hinge[b], Omar Wani[c*]

[a] *University of Alabama, Department of Geography and Environment, Tuscaloosa, 35401, AL, United States of America*
[b] *National Institute of Technology Durgapur, Department of Civil Engineering, Durgapur, 713209, West Bengal, India*
[c] *New York University, Tandon School of Engineering, Brooklyn, 11201, NY, United States of America*

Abstract

Nonlinear relationships between river discharge and flood inundation complicate effective flood risk assessments. In this study, we characterize the behavior of these nonlinearities. We explore the nature of the expected shifts in mean and variance of inundation due to various kinds of river discharge nonstationarities. Viewing flood inundations through the lens of Jensen's inequality, we show that the shifts in flood discharge do not result in proportionate shifts in inundation extent. We introduce a Jensen's Inundation Factor (JIF), which is an aggregate index dependent on the river-reach nonlinearity and the parameters of the discharge distribution. We highlight the implications of Jensen's inequality by running an operational NOAA OWP HAND flood inundation model across six catchments in the United States. Our results confirm a variety of nonlinear relationships across all basins, with critical discharge thresholds - providing insights that allow for more reliable flood risk estimation. We use these examples as a basis to highlight the need to understand river-reach level nonlinearities for evaluating climate nonstationarities - as global shifts in rainfall will not translate to proportionate shifts in inundation extent.

Keywords: Flooding, inundation extent, Jensen's inequality, nonlinearity, nonstationarity

---

1. Introduction

Flooding remains a formidable natural disaster, disrupting hydro-ecological systems and causing substantial socio-economic losses[1, 2]. In recent years, there has been a noticeable increase in the frequency and severity of fluvial, pluvial, and compound flooding events in many parts of the world[3, 4, 5, 6]. This surge in flooding events is characterized by the rise in floodwater levels that breach levees and inundate floodplains, causing flooding and damage in areas that were previously safe[7]. At the heart of this growing crisis is a confluence of factors: shifting climate, changing land use patterns, and rapid population growth[8, 9]. These factors exacerbate the impact of extreme weather events by altering the local hydrological cycle, leading to increased river discharge and heightened flood risks[7, 10]. Thus, gaining insight into the extent and patterns of the escalation in current flood levels is imperative for formulating resilient strategies in areas prone to vulnerability.

Traditionally, flood models have relied on stationary assumptions about input precipitation distributions, where past hydrological patterns/return period events are used to predict future flood risks[11]. However, this approach is becoming increasingly unreliable in the face of nonstationarity - the idea that river discharge patterns are evolving due to climate variability, land use changes, and human interventions [12, 13, 14]. Under nonstationarity, small changes in river discharge can result in various responses in inundation distributions, leading to amplification or damping of shifts [12]. Non-stationary conditions complicate flood predictions and challenge the effectiveness of current flood hazard maps because meaningfully assigning exceedance probabilities to various events becomes challenging[13]. Notably, in recent years, significant portions of flood insurance claims have originated outside the confines of regulatory flood hazard boundaries, drawing attention to the limitations of existing flood hazard maps. These maps have faced widespread criticism for presenting flood hazards as a binary process—within or outside inundation probability—while neglecting the inherent uncertainties in model estimates[15].

The present study aims to bridge this gap in understanding the combined effect of flood inundation nonlinearity and nonstationarity in river discharge. Armed with the mathematical concept of Jensen's inequality[16], this study explores the relationships that characterize this nonlinear behavior. Jensen's inequality, a fundamental principle in probability theory[17], provides insight into how the average behavior of a dependent random variable is in relation to the behavior induced by the average independent variable. The dependent random variable, in this case, is the flood inundation, while the stream flow is the independent random variable. We use systematic shifts in the streamflow distribution to see its influence on flood inundations. Through a suite of carefully designed simulation experiments, this investigation seeks to decipher the factors governing flood inundation expansion and intensity.

In particular, this study introduces the concept of the Jensen Inundation Factor (JIF), a numerical parameter that quantifies the damping and amplification in the flood inundation shifts relative to the shifts in the streamflow. By investigating how shifts in the mean of the discharge distribution impact inundation behavior using the National Oceanic and Atmospheric Administration - Office of Water Prediction (NOAA-OWP) operational Height Above the Nearest Drainage (HAND) based flood inundation model (FIM), the study offers a methodology with the potential to significantly enhance the precision and reliability of flood forecasting. This approach promises not only practical benefits for flood management but also contributes to the broader scientific discourse surrounding flood modeling, adaptation, and the intricate relationship between river discharge and inundation extent. Understanding these dynamics will help improve flood risk assessments, particularly in the face of increasingly unpredictable hydrological patterns driven by climate change.

2. Methods and material

2.1. Conceptual overview

2.1.1. Nonlinear transformations and Jensen's inequality

Nonlinear transformations are crucial for understanding how random variables are affected by nonlinear functions. Consider a random variable X representing river discharge. When this variable is transformed by a nonlinear function $f(x)$, the expected value of $f(X)$ is generally not equal to $f(\mathbb{E}[X])$. This discrepancy arises because nonlinear functions alter the distribution of X in ways that can either amplify or dampen the effect of changes in X on the transformed variable.

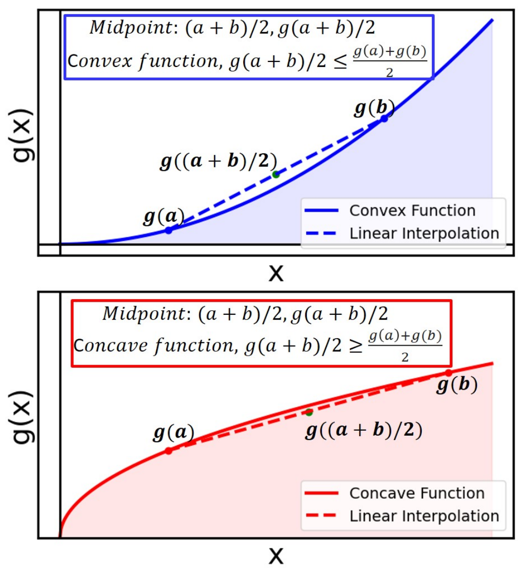

Figure 1: Convex and concave behavior of functions.

A function $g(x)$ is defined as convex if, for any two points a and b, the function value at the average of a and b is less than or equal to the average of the function values at a and b[18] (Figure 1) :

$$g\left(\frac{a+b}{2}\right) \leq \frac{g(a)+g(b)}{2} \tag{1}$$

Conversely, a function $g(x)$ is concave if the function value at the average of a and b is greater than or equal to the average of the function values at a and b(Figure 1) :

$$g\left(\frac{a+b}{2}\right) \geq \frac{g(a)+g(b)}{2} \tag{2}$$

Jensen's inequality relates to these definitions by stating that for a convex function $g(x)$ and a random variable X, the expected value of the function is greater than or equal to the function evaluated at the expected value of X[17]:

$$\mathbb{E}[g(X)] \geq g(\mathbb{E}[X]) \tag{3}$$

For concave functions $g(x)$, the inequality reverses:

$$\mathbb{E}[g(X)] \leq g(\mathbb{E}[X]) \tag{4}$$

2.1.2. Jensen's Inundation Factor - damping and amplification

Here we introduce Jensen Inundation Factor (JIF) to quantify the nonlinear relationship between inundation and river discharge. To account for non-stationarity in streamflow, USGS gauge discharge data is fitted with a log-normal distribution and then adjusted with systematic multipliers. The JIF is calculated as follows:

$$\text{JIF} = \frac{\mathbb{E}[g(X)]}{g(\mathbb{E}[X])} \tag{5}$$

where $g(\mathbb{E}[X])$ is the value of the function g evaluated at the expected value of X and $\mathbb{E}[g(X)]$ is the expected value of the function $g(X)$ when applied to X.

The curve in Figure 2 represents the nonlinear relationship between river discharge and flood inundation extent. At lower discharge (within bankfull), the relationship appears relatively linear, with a gradual increase in inundation. As discharge approaches and exceeds bankfull, the curve bends more sharply, reflecting a nonlinear response where inundation increases more dramatically. In reality, the shape of the curve varies, and for different topographies, it bends with different shapes and slopes. Convex sections (red dashed line) indicate a rapid increase in inundation, while concave sections (green dashed line) show a slower rise in inundation extent. The curve highlights how different landscapes and discharge scenarios influence flood risk. This concept aligns with Jensen's Inundation Factor, which quantifies the nonlinear relationship between inundation and streamflow.

Various values of JIF, which signify damping and amplification, are used to indicate the disproportionality of the change in inundation with respect to the change in streamflow. Specifically, damping occurs when the shift in inundation is less than the relative shifts in streamflow, indicating a lower inundation response to discharge shifts. This damping phenomenon is a result of a sublinear response to the shifts in streamflow. In contrast, amplification reflects that the shifts in inundation is higher relative to the shift in the streamflow, signifying a more pronounced flood response. The amplification phenomenon is a result of the superlinear response to the shifts in streamflow. For sublinear response, JIF is less than 1 and for superlinear response JIF is greater than 1.

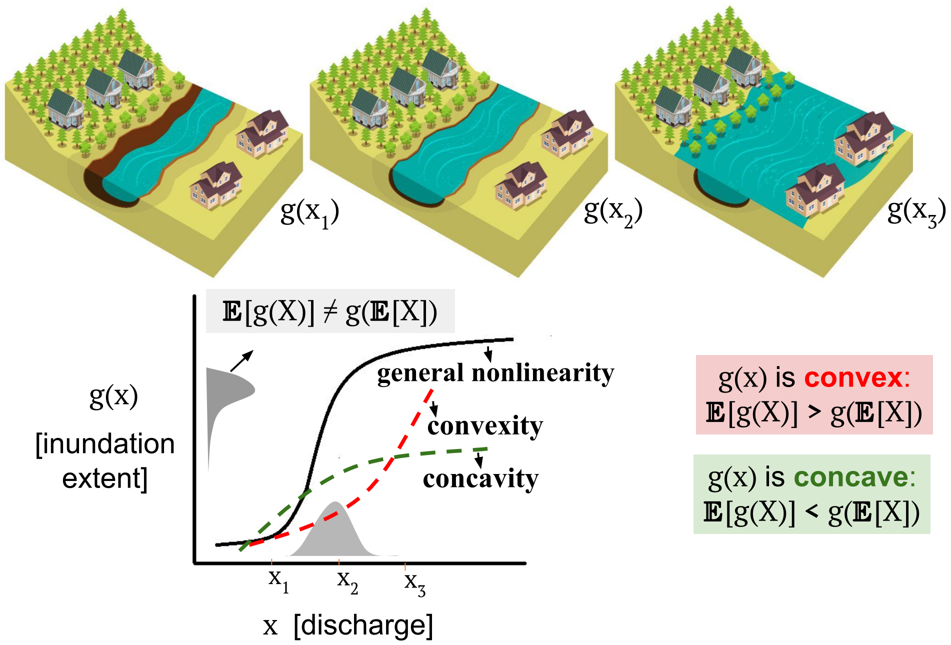

Figure 2: Conceptualization of Jensen's inequality for different discharge-inundation nonlinearities

2.1.3. Proof of concept - analytical derivation

The simplest way to express the discharge-inundation nonlinearity in fluvial flooding is by using Manning's equation. It is used to estimate the discharge at a given time based on the hydraulic geometry and river slope. Although it is for uniform flow, it is representative of the nonlinear relationship between the stream flow and flood inundation.

The Manning's-Stickler equation in open channel flow is expressed as:

$$Q = A \cdot \left(\frac{1}{n} R^{2/3} S^{1/2} \right) \tag{6}$$

where $R = \frac{A}{P}$. P is the wetted perimeter. Therefore:

$$Q = k \cdot A^{5/3} P^{2/3} \tag{7}$$

For a triangular section, $A = \frac{Ih}{2}$, where I is the top width of the section and h is the flow depth from the bottom.

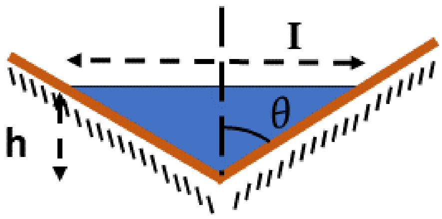

Figure 3: Simple triangular section used for geometric illustration in the derivation of Manning's equation

From simple geometric considerations for a triangular channel (Figure 3) :

$$h = I \tan\left(\frac{\theta}{2}\right) \tag{8}$$

$$A = \frac{I^2 \tan^2\left(\frac{\theta}{2}\right)}{2} \tag{9}$$

$$P = I \sin(\theta) \tag{10}$$

Substituting A and P into the equation for Q:

$$Q = k \cdot (\sin(\theta))^{2/3} \cdot \left(\frac{\tan^2\left(\frac{\theta}{2}\right)}{2}\right)^{5/3} \cdot \left(I \cdot \frac{\sin(\theta)}{\tan\left(\frac{\theta}{2}\right)}\right)^{2/3} \tag{11}$$

Simplifying, we get:

$$I^{\frac{8}{3}} = \frac{Q}{K'} \tag{12}$$

$$I = K \cdot Q^{\frac{3}{8}} \tag{13}$$

Let X be a random variable representing discharge, following a uniform distribution between 0 and b, where b is the highest flow :

$$X \sim U_{[0,b]} \tag{14}$$

The probability density function is:

$$p_X(x) = \frac{1}{b} \tag{15}$$

Now, let $Y = g(X)$. The nonlinear transform of Y is:

$$p_Y(y) = p_X(x) \cdot |\frac{d(g^{-1}(y))}{dy}| \tag{16}$$

Substituting:

$$g^{-1}(y) = \left(\frac{y}{c}\right)^{\frac{8}{3}} \tag{17}$$

$$\frac{d\left(\frac{y}{c}\right)^{\frac{8}{3}}}{dy} = \frac{8}{3}\left(\frac{y}{c}\right)^{\frac{5}{3}} \tag{18}$$

From equations (15) and (16), we get:

$$p_Y(y) = \frac{1}{b} \cdot \frac{8}{3} \cdot \left(\frac{y}{c}\right)^{\frac{5}{3}} \tag{19}$$

Now, calculating the expectation:

$$\mathbb{E}[X] = \int_0^b x \cdot p_X(x)\,dx = \int_0^b \frac{x}{b}\,dx = \frac{b}{2} \tag{20}$$

Now:

$$\mathbb{E}[g(X)] = \mathbb{E}[Y] = \int_0^{cb^{\frac{3}{8}}} y \cdot p_Y(y)\,dy \tag{21}$$

Further integrating, we get:

$$\mathbb{E}[g(X)] = \frac{8}{11} \cdot \frac{c}{b^{\frac{3}{8}}} \tag{22}$$

Using equation (13), which represents the nonlinearity in a triangular channel:

$$g(\mathbb{E}[X]) = c\left(\frac{b}{2}\right)^{\frac{3}{8}} = \frac{c}{2^{\frac{3}{8}}} \cdot b^{\frac{3}{8}} \tag{23}$$

Dividing equations (22) and (23):

$$\frac{\mathbb{E}[g(X)]}{g(\mathbb{E}[X])} = \frac{\frac{8}{11} \cdot c \cdot b^{\frac{3}{8}}}{\frac{c}{2^{\frac{3}{8}}} \cdot b^{\frac{3}{8}}} = 0.943 \tag{24}$$

This is one of the simplest analytical demonstrations of Jensen's inequality for flood inundation with increasing discharge. The JIF < 1 represents the damping effect in inundation shifts as the discharge distribution shifts towards the right. As the water level rises, the velocity in the channel also increases, allowing more water to pass through the same cross-sectional area. As a result, the inundation extent does not increase proportionately to the increase in discharge.

2.1.4. Climatic and topographical influence on Jensen's Inundation Factor

Let X be the input random variable with probability distribution function $p_X(x \mid \theta)$, where θ is the set of parameters determining its location, shape, and scale.

Given $g(x, \Psi)$ is the non-linearity, with parameters Ψ, the expectation is given by:

$$\mathbb{E}[g(X, \Psi)] = \int_{-\infty}^{\infty} g(x, \Psi) p_X(x \mid \theta)\, dx = f_1(\Psi, \theta) \tag{25}$$

where $f : \mathbb{R}^n \to \mathbb{R}$ represents any general functional relationship from the n-dinemsional parameter space to real line.

Similarly:

$$g(\mathbb{E}[X]) = f_2(\Psi, \theta) \tag{26}$$

which leads to

$$\text{JIF} = \frac{\mathbb{E}[g(X)]}{g(\mathbb{E}[X])} = \frac{f_1(\Psi, \theta)}{f_2(\Psi, \theta)} = f_3(\Psi, \theta) \tag{27}$$

This equation shows that the JIF factor is dependent on both the parameters of the nonlinear relationship and the parameters of the distribution of the discharge. While the function $g(x)$ remains constant for a given catchment property, the parameters θ can change due to non-stationarity in the input time series. This non-stationarity may arise from factors such as climate variability, land use changes, and alterations in hydrological processes, leading to complex interactions within the hydrological system.

Climate significantly affects the parameters θ within the distribution of X. Variations in precipitation patterns and extreme weather events can alter the flow characteristics of a catchment area. For example, increased rainfall intensity may lead to higher peak flows, thereby impacting the relationship between discharge and inundation. Conversely, prolonged drought conditions can reduce soil moisture and modify runoff patterns, affecting the frequency and distribution of flood events.

Topographical features, including slope, elevation, and drainage density, also play a crucial role in shaping hydrological responses within a catchment. The land surface's geometry influences how water moves across the landscape, which affects both the timing and magnitude of runoff. Steeper slopes may result in faster runoff and reduced infiltration, while flatter areas may facilitate greater water retention and slower flow. This interplay between climatic and topographical factors can create complex responses in flood behavior. In regions with diverse topography, the spatial distribution of rainfall can lead to heterogeneous flood responses. Steep terrain might experience rapid runoff and localized flooding, whereas low-lying regions may be more susceptible to prolonged inundation.

In summary, while $g(x)$, the inundation response for a given stream flow, is primarily governed by the inherent properties of the catchment, like its morphology, Jensen's Inundation Factor is influenced by both climatic and topographical variables. The introduction of non-stationarity due to changing land use and climate significantly alters the hydrological dynamics of a region. Understanding these influences is crucial for effectively modeling flood inundation, particularly in the context of ongoing climate change and urbanization.

2.2. Simulation experiments

The overall methodology for the case studies is shown in Figure 4.

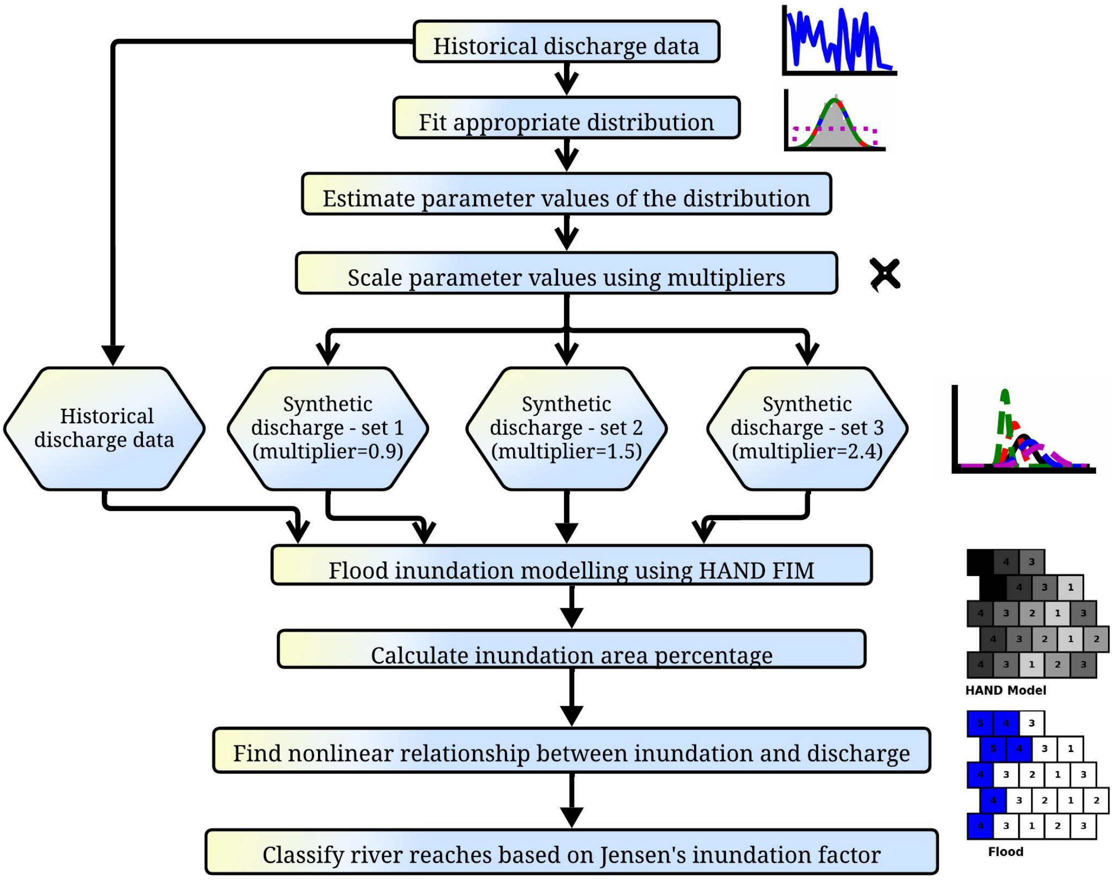

Figure 4: Overall methodology for the Case studies

2.2.1. Study area

The study area includes six catchments located across the United States: Upper Neuse, Middle Neuse, Upper Saline, Lake Conway, Rio-Granade Santa Fe, and Ouachita Headwaters (Figure 5). These catchments were selected to represent diverse hydrological and geographical characteristics. The Upper Neuse and Middle Neuse catchments, located in North Carolina, are characterized by steep topography and mixed land use, including forest, urban, and agricultural areas[1]. The Upper Saline catchment in Arkansas is characterized by predominantly rural land use and varied topography, including mountainous terrains. Lake Conway, in Arkansas, is situated in a low-lying coastal plain with significant urbanization around the lake area. The Ouachita Headwaters catchment, spanning Arkansas and Oklahoma, is characterized by diverse land use and relatively steep topography. This selection of catchments allows for a comprehensive analysis of the impact of river discharge nonstationarity on flood inundation extents across different geographical and hydrological settings.

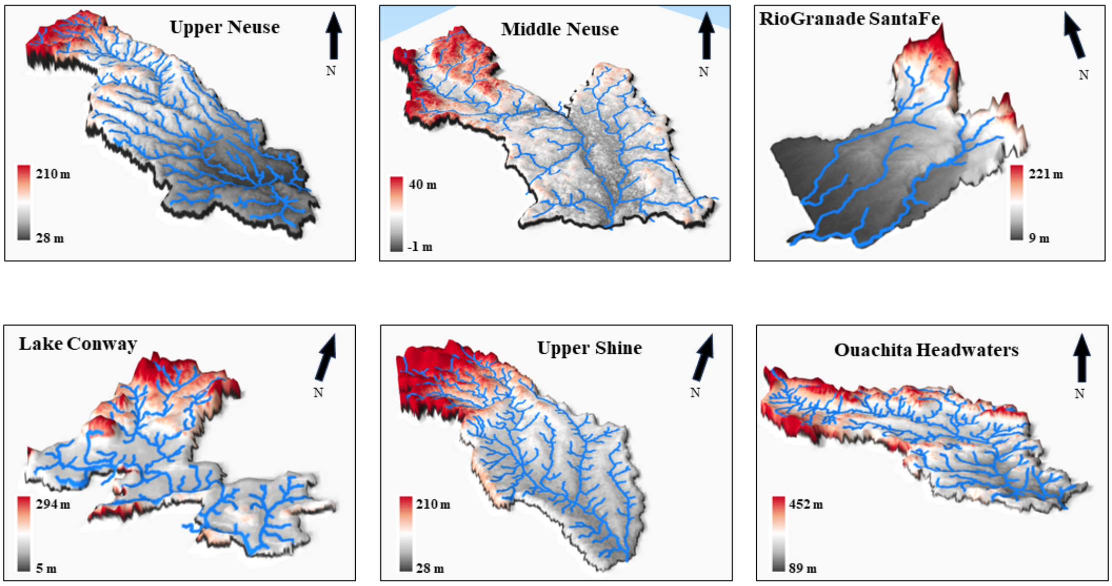

Figure 5: Study area showing the six catchments across the United States.

2.2.2. Discharge data

United States Geological Survey (USGS) gauge discharge data for 20 years are used for these six selected catchments(https://waterdata.usgs.gov/nwis?).This hydrological data set included long-term historical river discharge records available on daily interval. These records were crucial for understanding the variability and characteristics of river flow in each catchment.

2.2.3. Synthetic discharge generation

Statistical analysis was performed to determine the best probability distribution that fits with the discharge data collected for each catchment. For all six catchments, we used the lognormal distribution as the best fit. This choice was guided by the statistical properties of river discharge data, which often exhibit skewness and heavy tail — characteristics well-captured by the Lognormal distribution [19, 20]. The Lognormal distribution is defined as follows:

$$f(x \mid \mu, \sigma) = \frac{1}{x\sigma\sqrt{2\pi}} \exp\left(-\frac{(\ln x - \mu)^2}{2\sigma^2}\right) \tag{28}$$

where μ is the location parameter of and σ is the shape parameter of the log-normal distribution

For discharge shifts, we generated synthetic samples with the following process:

Step 1: Calculation of parameters: For each catchment, the parameters of the stream flow time series were estimated using maximum likelihood estimation. In log-normal distributed stationary time series, the mean and standard deviations are the best representative of the location μ and scale σ parameters. These parameters provide a statistical basis for subsequent simulations.

Step 2: Discharge shift:The calculated parameters from the gauge data (μ and σ) are multiplied with different factors to implicate various discharge shifting scenarios. These factors are random (0.9,1.5, and 2.4), which adjusted the original distribution parameters to reflect different discharge scenarios. These shifts are implemented to generate various discharge scenarios, a potential indicator of climate change impacts, land use alterations, urbanization, and hydrological modifications. By applying these shifts, we generated synthetic discharge values that allowed for a comprehensive evaluation of how changes in river flow affect flood inundation across different catchments. These new parameters represent shifts in the variability and mean of the discharge.

Step 3: Generation of synthetic data: For each case study, we calculated new parameters (μ_{new},and σ_{new}) as shown below:

$$\mu_{\text{new}} = \text{factor} \times \mu \tag{29}$$

$$\sigma_{\text{new}} = \text{factor} \times \sigma \tag{30}$$

where μ and σ are the original location and scale parameters, while μ_{new} and σ_{new} are the new parameters used to generate the synthetic discharge data. These synthetic discharge time series are then used to simulate various flood conditions and assess the impact of different discharge scenarios on flood inundation.

2.2.4. Flood inundation mapping and percent flooding calculation

The NOAA-OWP HAND FIM (Height Above the Nearest Drainage - Flood Inundation Mapping) is used to simulate flood inundation extents for various scenarios across all six catchments[21].OWP HAND-based FIM is a continental-scale flood inundation model capable of producing flood depth and inundation extents at high spatial and temporal resolution. The model runs at 10m resolution 3DEP elevation products with hourly national water model (NWM) retrospective and forecasted streamflow.The model uses Manning's equation to construct reach-averaged synthetic rating curves for the entire watershed (HUC-8) using the reach-averaged cross-sectional parameters. The HAND-derived synthetic rating curves (SRCs) provide the key piece of information needed to convert an input streamflow value (NWM retrospective/forecast streamflow) into the corresponding HAND stage value. This stage-discharge relationship facilitates the production of flood inundation maps (FIMs) . If the stage for a given discharge is higher than the relative elevation, water spills into the floodplains or vice versa. Although this framework does not account for mass and momentum conservation or solve the Saint-Venant Equations, its scalability and low computational cost make it suitable for large-scale simulations [22]

Manning's equation is given by:

$$Q = A \cdot \frac{1}{n} \cdot R^{2/3} \cdot S_0^{1/2} \tag{31}$$

where Q is the discharge, A is the cross-sectional area, n is the Manning's roughness coefficient, R is the hydraulic radius, and S_0 is the slope of the flow.

The OWP HAND FIM flood model runs at the watershed scale, including the headwater streams. Being computationally efficient, the model can produce 10m resolution flood maps at HUC-8 scale watersheds in less than a minute. The model was configured to run automatic simulations for all six basins under four different scenarios: one using gauge discharge data and three with shifted discharge datasets (0.9, 1.5, and 2.4). Each scenario produced 100 binary flood rasters, resulting in a total of 2,400 samples. In this case, we ran the model multiple times, and to make the computation less tedious, we focused on major streams having a stream order higher than 4. Using these simulated flood inundation extents, we calculated the percentage of flooding for each scenario based on the binary flood maps.For each scenario i, the flood inundation percentage (P_i) is calculated as:

$$P_i = \frac{\text{Number of Flooded Pixels}}{\text{Total Number of Pixels}} \times 100 \tag{32}$$

Percent inundation extents are plotted against the river discharge to analyze the relationship between flood percentage and discharge. This analysis aimed to identify whether the relationship was linear, sub-linear, or super-linear across the different catchments.

2.2.5. Application of Jensen's inequality and JIF

Jensen's inequality and Jensen's Inundation Factor (JIF) are crucial for analyzing the nonlinear relationships between river discharge and flood inundations. These concepts, thoroughly explained in Sections 2.1 and 2.2, are applied to assess how nonlinear transformations impact flood predictions.

Jensen's inequality provides a framework to understand how the expected value of a nonlinear function of a random variable, such as river discharge, differs from the nonlinear function of the expected value. This is particularly relevant for flood modeling because river discharge often exhibits complex, nonlinear behavior. By applying Jensen's inequality, it is possible to evaluate whether flood inundation is more or less sensitive to changes in discharge than would be predicted by a simple linear model.

The Jensen's Flood Inundation Factor (JIF) extends this analysis by quantifying the degree of nonlinearity in the relationship between streamflow and flood extent. JIF is calculated by comparing the expected value of the nonlinear function of discharge to the function evaluated at the expected value of discharge. This factor provides insights into whether flood inundation indicates damping or amplification effects in response to variations in river discharge.

3. Results and discussion

3.1. Discharge and inundation distributions across various basins

To analyze the relationship between river discharge and flood inundation, we employed a series of parameter shifts as described in the methodology. .

Figure 6 shows the frequency of discharge and inundation across various basins using observed and synthetic discharge values. A significant change in discharge values was observed after shifting the distribution parameters. For instance, in the Upper Neuse, the maximum observed discharge is approximately 254 m^3/s, while with the synthetic discharge values, the maximum value from our sample set reaches 600 m^3/s. The percent of inundation increases as we move from the gauge discharge towards the 2.4 shifted scenarios by an amount of 40%. From this scenario analysis, we found that even after there is a substantial change in the discharge (in this case, different synthetic discharge scenarios) potentially attributed to climate change, land use alterations, urbanization, or hydrological modifications, there is no significant flood inundation we observed for the Upper Neuse basin. The relationship we observed is sublinear between the discharge-inundation, where even the extreme shifts in discharge lead to a minor increase in inundation from the actual inundation(0.1% to 0.17%).

In the Middle Neuse catchment, gauged discharge values range from 0.17 to 257 m^3/s, with maximum shifting we get the maximum discharge of 800 m^3/s. Similar to the Upper Neuse, the frequency of inundation shows a considerable increase across synthetic discharge scenarios, where inundation percentages increase from 4% to nearly 24%. This indicates that the Middle Neuse catchment is also sensitive to changes in discharge values and shows a nonlinear relationship between discharge and inundation extent. Conversely, the Rio Grande Santa Fe shows a consistently lower discharge distribution, with gauged discharge ranging from 2 to 70 m^3/s. The response of inundation to synthetic discharge shifts is less pronounced here, with inundation percentages increasing only from 5% to 25%. This suggests that the Rio Grande Santa Fe catchment may have a lower sensitivity to discharge changes, indicating a potentially more resilient hydrological response compared to the other basins analyzed while still showing nonlinear dynamics in the relationship between discharge and inundation.

The Lake Conway catchment presents a broad discharge distribution, with observed values from 0.25 to 110 m^3/s, and the maximum shift in synthetic discharges is 311%.

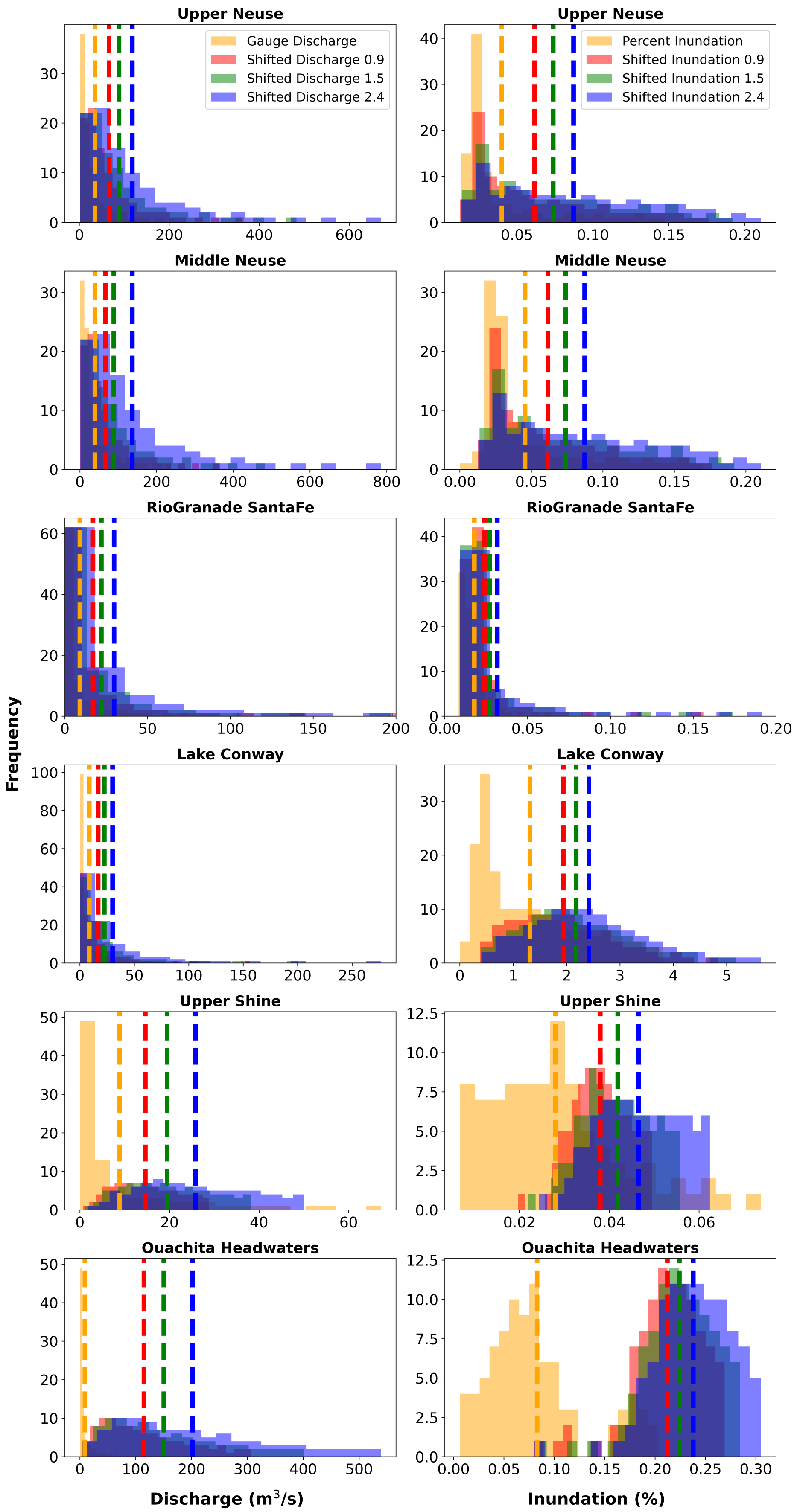

Figure 6: Comparison of actual and synthetic discharge frequency across various basins and scenarios

In this basin, the frequency of inundation dramatically increases, particularly with 2.4 scenerio, where inundation percentages increase to over 45%. The Upper Shine basin shows a narrower discharge distribution, with observed values ranging from 0.009 to 65 m^3/s, and after shifting, the maximum discharge value is $121 m^3/s$. Despite this increase in discharge, the inundation percentage increased to 35%.

Lastly, the Ouachita Headwaters show a diverse discharge distribution, with observed values from 0.25 m^3/s to 117 m^3/s and synthetic discharges reaching up to a maximum value of 550 m^3/s. Notable increases in inundation frequency are evident, particularly at the highest discharge values, with inundation percentages rising to 51%. This observation underscores the non-linear relationship between discharge and inundation, consistent with the patterns observed in all the other five basins.

3.2. Discharge-inundation dynamics across river basins

Building on the observations from Section 4.1, discharge versus inundation is plotted to further clarify how the relationships between discharge and inundation extents across different basins based on 100 simulations for each basin and each scenario, presented in both normal and semi-logarithmic scales, as shown in Figure 7. It can be seen that overall, all catchments show a nonlinear and predominantly sub-linear trend. However, some catchments initially display a linear response to increases in discharge, transitioning to a sub-linear trend after reaching a specific threshold. Others show a super-linear trend at lower discharge values before shifting to a sub-linear trend.

In the Upper Neuse Basin, a significant increase in inundation occurs at discharge levels of approximately 150–200 m^3/s, marking a critical threshold where small increases beyond this point can lead to much greater flooding. The Middle Neuse Basin also shows a notable rise in inundation once discharge levels exceed 200 m^3/s, emphasizing its sensitivity beyond this discharge value.

In contrast, the Rio Grande Santa Fe Basin presents a more linear trend, appearing relatively straight throughout its range, indicating a consistent relationship between discharge and inundation levels. This pattern is echoed in the Lake Conway Basin, which similarly exhibits a gradual rise starting at comparable discharge levels. The Upper Shine Basin displays a steady increase in inundation up to 30–40 m^3/s, followed by a sharper rise, suggesting that minor changes in discharge can have a considerable impact. Finally, the Ouachita Headwaters Basin experiences a gradual rise in inundation up to 200 m^3/s, after which the trend shifts, particularly indicating a transition from sub-linear to super-linear behavior as discharge crosses 80 m^3/s.

The observed variability across the basins reveals the intricate dynamics of how each basin responds to fluctuations in discharge levels. Understanding these distinct trends is crucial for developing effective flood risk management strategies, as it allows for tailored approaches that account for the unique hydrological behaviors of each basin.

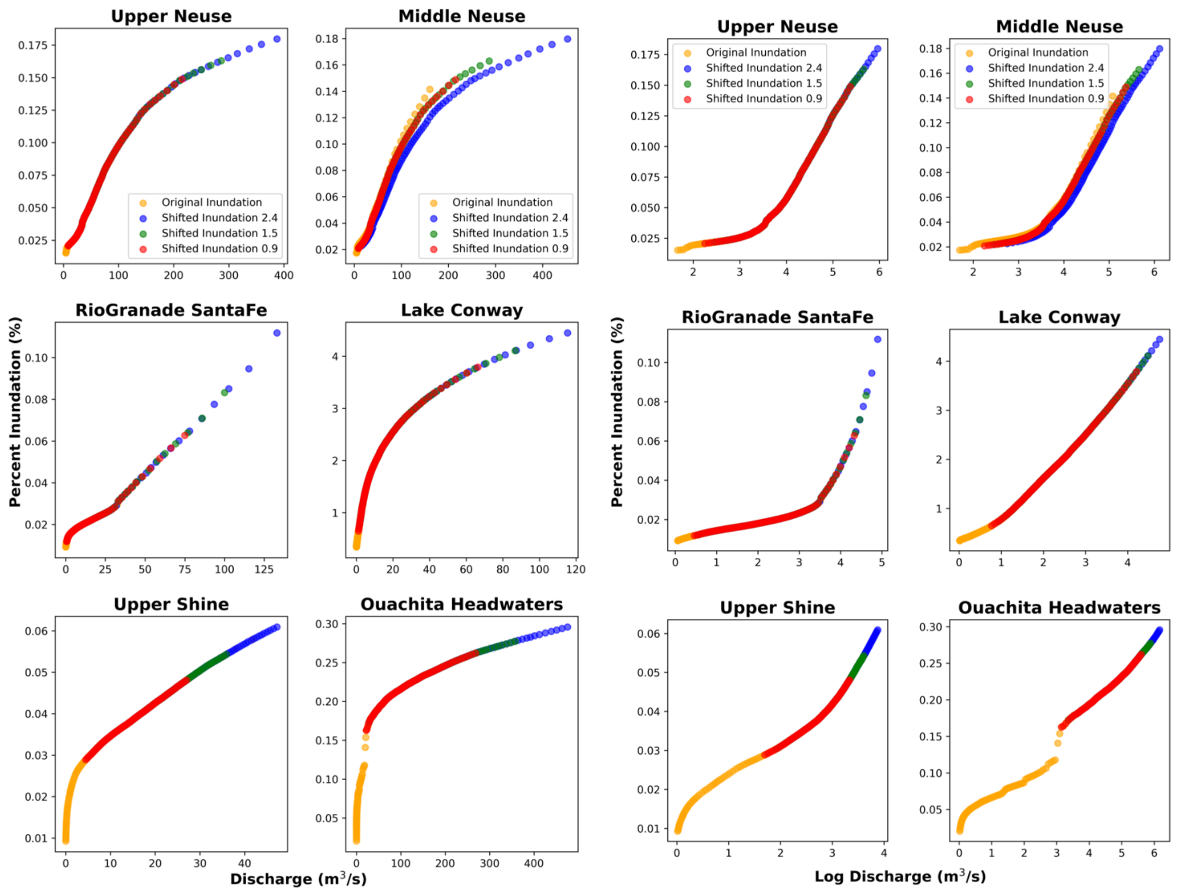

Figure 7: Relationship between discharge (m^3/s) and percent inundation for various river basins, illustrated through linear scales (first and second columns) and semi-logarithmic scales (third and fourth columns)

3.3. Analyzing JIF

JIF for the different basins under various discharge scenarios as shown in Table 1 reveal important patterns regarding flood inundation dynamics. It provides insights into the non-linear responses of each basin to changes in discharge and highlights the differential impact of flood events across different basins.

The Upper Neuse and Middle Neuse basins were found to have higher JIF values across all scenarios, particularly under the original and shifted 0.9 discharge scenarios, with values of 0.98 and 0.97, respectively, in the original scenario and 0.85 and 0.86 in the shifted 0.9 scenario. However, as the discharge shifts further to 1.5 and 2.4 scenarios, the JIF values gradually decrease, indicating a sub-linear flood response. This trend indicates that, despite increasing discharge values, the flood extent in these basins does not increase proportionally, likely due to the presence of better drainage systems or resilient topographical features.

In contrast, the Rio Grande Santa Fe basin is more sensitive to discharge increases. Its JIF value drops from 0.86 in the original scenario to 0.62 under the shifted 2.4 discharge scenario. A JIF value below 1 typically reflects a sublinear relationship between discharge

Table 1: Jensen's Inundation Factor for different basins.

Basin	**Scenarios**			
	Original	**Shifted_0.9**	**Shifted_1.5**	**Shifted_2.4**
Upper Neuse	0.98	0.85	0.80	0.78
Middle Neuse	0.97	0.86	0.81	0.78
RioGranade SantaFe	0.86	0.84	0.76	0.62
Lake Conway	0.71	0.67	0.75	0.72
Upper Shine	0.83	0.99	0.99	0.98
Ouachita Headwaters	0.85	0.96	0.96	0.96

and inundation extent, meaning that as discharge increases, the extent of flooding is increasing very gradually. However, this substantial drop signifies a shift in how the basin manages excess water, suggesting that extreme discharge scenarios may lead to less severe flooding than expected. The decline indicates a tipping point in the basin's capacity, implying that while incremental increases in discharge may not cause significant flooding, the overall effectiveness in handling larger discharges is declining. The vulnerability of the Rio Grande Santa Fe basin may also stem from its topographical characteristics, as flatter areas often have less capacity to convey water away, leading to greater inundation extents when discharge increases significantly. With elevations ranging from 9 to 221 meters, the presence of only a small higher elevation area may limit the basin's ability to effectively manage excessive runoff, especially during extreme discharge events.

The Lake Conway basin shows a distinct characteristic compared to the others, with relatively lower JIF values across all scenarios, beginning at 0.71 in the original discharge scenario. Interestingly, the JIF increases slightly to 0.75 under the shifted 1.5 scenario before slightly decreasing again to 0.72 under the shifted 2.4 scenario. This fluctuating pattern could be due to Lake Conway's urban or semi-urban characteristics, where even small shifts in discharge can trigger significant changes in flood extent. The basin's elevation ranges from 5 to 224 meters, with a majority of areas at higher elevations, suggesting that topographical features may influence its flood response. However, despite these higher elevations, certain flatter regions may limit the efficient movement of excess water during flood events, indicating a vulnerability to flooding.

The Upper Shine and Ouachita Headwaters basins show relatively stable JIF values across all discharge scenarios. Both basins consistently show JIF values above 0.96 but below 1, indicating a nearly linear or slightly sub-linear relationship between discharge and flood extents. This suggests that increasing discharge does not significantly impact flooding in these areas. The Upper Shine basin, with elevations ranging from 28 to 210 meters and predominantly higher elevation areas, along with the Ouachita Headwaters basin, which ranges from 89 to 452 meters and has significant portions at higher elevations, likely benefits from their topography. This higher elevation landscape enhances their capacity to manage excess discharge effectively, resulting in a stable flood extent even as discharge values increase.

Thus, while the flood inundation extent consistently increases with discharge, the rate of increase and the mean inundation, given the distribution of flow, are influenced by flow probability parameters and nonlinearity factors. The introduction of the novel Jensen's Inundation Factor (JIF) in this paper offers valuable insights into the flood response of different basins. Changes in JIF values indicate that as discharge increases, the relationship between discharge and flood inundation becomes more complex. Thus, JIF introduced here can provide a clearer understanding of the dynamics of flood inundation across various basins. By identifying basins that may be more susceptible to flooding under increased discharge scenarios using JIF, policymakers can prioritize areas for infrastructure improvements and apply mitigation strategies.

3.4. Insights and implications for future studies

A major insight from this study is the nonlinear relationship between shifts in precipitation and the associated inundation extent, primarily influenced by complex interactions within diverse landscapes. This finding underscores the necessity of considering shifts in precipitation when assessing flood risks as well as critical factors such as the Jensen Inundation Factor (JIF). The JIF provides a nuanced understanding of inundation dynamics, indicating that inundation extent or flood risk does not scale directly with precipitation; instead, landscape features act as amplifiers or dampers, significantly affecting the extent and intensity of flooding.

Incorporating the JIF into our model allows us to account for variable responses of different basins to changes in precipitation volume, particularly with different basins characterized by diverse topographic features. The observed nonlinear dynamics challenge conventional flood risk estimates that typically assume a proportional relationship between precipitation and flooding. Our findings indicate that regions experiencing similar precipitation changes may face disparate flood risks shaped by their unique landscape characteristics.

The implications of this study advocate for a transformative shift in flood risk modeling and urban development strategies within flood-prone regions. Resilience planning must incorporate these nonlinear flood responses to better anticipate the impacts of even modest increases in precipitation. By employing the JIF in risk assessments, urban developers and policymakers can effectively identify areas vulnerable to heightened flooding and prioritize adaptive infrastructure or natural buffers.

In the context of a rapidly changing climate, where precipitation patterns are increasingly erratic, integrating the JIF or similar metrics into flood risk assessments fosters a more targeted approach to flood resilience. Rather than treating flood risk as a direct function of precipitation alone, this framework accounts for localized landscape responses, guiding the formulation of policies that fortify vulnerable regions. Through this lens, flood risk management evolves into a more adaptive and nuanced process, congruent with the intricate nature of natural landscapes, ultimately enabling the development of more effective flood protection strategies for communities facing climate-driven flood intensification.

4. Conclusion

Our study highlights the effect of nonlinearity between flood inundation extent and river discharge on flood risk assessments. Our findings suggest that an increase in discharge due to increased precipitation alone will not necessarily lead to a proportional increase in inundation extent. Instead, the introduction of Jensen's Inundation Factor reveals that various nonlinear dynamics, including damping and amplification mechanisms, significantly influence the flood behavior of a catchment, influenced by factors such as topography, climatology, and hydrodynamics.

Our analysis emphasizes that the anticipated increase in flood inundation is usually not a linear function of flood discharge. Local hydrological conditions and catchment characteristics can significantly attenuate or amplify the relationship between precipitation and flood extent in these catchments. While, for the six analyzed catchments, we observed only damping effects in inundation shifts, other catchments around the world may exhibit either damping or amplification depending on specific local conditions. This variability emphasizes the necessity for context-specific evaluations, as the interplay between topography and hydrodynamics can influence flood inundation outcomes and the severity of damage.

Thus, future studies should focus on systematically identifying and classifying these nonlinearities across all populated reaches of major rivers and identifying critical thresholds related to flood risk. Understanding these thresholds will be essential for determining when specific catchments are likely to experience significant flooding under varying conditions. This classification will be crucial for informing policy decisions related to flood management and insurance claims, ultimately aiming to enhance community resilience against flooding.

This work, particularly the introduction of JIF, provides a theoretical framework for a desirable global analysis that would characterize flooding nonlinearities and summarize the interplay of nonlinear hydrological responses and climatic conditions by using a single index. As populations continue to grow in flood-prone areas, quantifying Jensen's Inundation Factor will be valuable for risk assessment and, in turn, for improving community preparedness.

Authorship contribution statement

Anupal Baruah: Ideas, simulation, writing, reviewing, and editing. **Gilbert Hinge**: Ideas, simulation, writing, reviewing, and editing. **Omar Wani**: Primary conceptualization and supervision. Statistical analysis, writing, reviewing, and editing

Data Availability Statement: The USGS gauge data can be accessed from https://waterdata.usgs.gov/nwis. The OWP HAND model can be accessed from https://github.com/NOAA-OWP/inundation-mapping. The Digital Elevation Model (DEM) used in this study is sourced from USGS.

Acknowledgements: We thank Candace Chow and Dipsikha Devi for their valuable comments.

Conflicts of Interest: The authors declare no conflict of interest.

References

[1] S. Zhang, L. Zhou, L. Zhang, Y. Yang, Z. Wei, S. Zhou, D. Yang, X. Yang, X. Wu, Y. Zhang, et al., Reconciling disagreement on global river flood changes in a warming climate, Nature Climate Change 12 (12) (2022) 1160–1167.

[2] J. Teng, A. J. Jakeman, J. Vaze, B. F. Croke, D. Dutta, S. Kim, Flood inundation modelling: A review of methods, recent advances and uncertainty analysis, Environmental modelling & software 90 (2017) 201–216.

[3] C. Wasko, R. Nathan, L. Stein, D. O'Shea, Evidence of shorter more extreme rainfalls and increased flood variability under climate change, Journal of Hydrology 603 (2021) 126994.

[4] A. Ionno, R. Arsenault, M. Troin, J.-L. Martel, F. Brissette, Impacts of climate change on flood volumes over north american catchments, Journal of Hydrology 630 (2024) 130688.

[5] G. Dharmarathne, A. Waduge, M. Bogahawaththa, U. Rathnayake, D. Meddage, Adapting cities to the surge: A comprehensive review of climate-induced urban flooding, Results in Engineering (2024) 102123.

[6] I. Mallakpour, G. Villarini, The changing nature of flooding across the central United States, Nature Climate Change 5 (3) (2015) 250–254. doi:10.1038/nclimate2516.
URL `https://ideas.repec.org/a/nat/natcli/v5y2015i3d10.1038`$_nclimate2516.html$

[7] Y. Hirabayashi, R. Mahendran, S. Koirala, L. Konoshima, D. Yamazaki, S. Watanabe, H. Kim, S. Kanae, Global flood risk under climate change, Nature climate change 3 (9) (2013) 816–821.

[8] R. Eccles, H. Zhang, D. Hamilton, R. Trancoso, J. Syktus, Impacts of climate change on streamflow and floodplain inundation in a coastal subtropical catchment, Advances in Water Resources 147 (2021) 103825.

[9] L. Stein, M. P. Clark, W. J. Knoben, F. Pianosi, R. A. Woods, How do climate and catchment attributes influence flood generating processes? a large-sample study for 671 catchments across the contiguous usa, Water Resources Research 57 (4) (2021) e2020WR028300.

[10] Z. W. Kundzewicz, S. Kanae, S. I. Seneviratne, J. Handmer, N. Nicholls, P. Peduzzi, R. Mechler, L. M. Bouwer, N. Arnell, K. Mach, et al., Flood risk and climate change: global and regional perspectives, Hydrological Sciences Journal 59 (1) (2014) 1–28.

[11] B. Merz, S. Basso, S. Fischer, D. Lun, G. Blöschl, R. Merz, B. Guse, A. Viglione, S. Vorogushyn, E. Macdonald, et al., Understanding heavy tails of flood peak distributions, Water Resources Research 58 (6) (2022) e2021WR030506.

[12] T. R. Kjeldsen, H. Kim, C.-H. Jang, H. Lee, Evidence and implications of nonlinear flood response in a small mountainous watershed, Journal of Hydrologic Engineering 21 (8) (2016) 04016024.

[13] S. Han, L. Slater, R. L. Wilby, D. Faulkner, Contribution of urbanisation to non-stationary river flow in the uk, Journal of Hydrology 613 (2022) 128417.

[14] H. Wang, W. Yuan, H. Yang, F. Hong, K. Yang, W. Guo, The ecological–hydrological regime of the han river basin under changing conditions: The coupled influence of human activities and climate change, Ecohydrology (2024).

[15] M. K. Buchanan, M. Oppenheimer, R. E. Kopp, Amplification of flood frequencies with local sea level rise and emerging flood regimes, Environmental Research Letters 12 (6) (2017) 064009.

[16] J. L. W. V. Jensen, Sur les fonctions convexes et les inégalités entre les valeurs moyennes, Acta mathematica 30 (1) (1906) 175–193.

[17] N. N. Taleb, Statistical consequences of fat tails: Real world preasymptotics, Epistemology, and Applications: Papers and Commentary (2020).

[18] N. N. Taleb, J. West, Working with convex responses: Antifragility from finance to oncology, Entropy 25 (2) (2023) 343.

[19] M. C. Bowers, W. Tung, J. Gao, On the distributions of seasonal river flows: lognormal or power law?, Water Resources Research 48 (5) (2012).

[20] A. G. Blum, S. A. Archfield, R. M. Vogel, On the probability distribution of daily streamflow in the united states, Hydrology and Earth System Sciences 21 (6) (2017) 3093–3103. doi:10.5194/hess-21-3093-2017.

[21] A. D. Nobre, L. A. Cuartas, M. Hodnett, C. D. Rennó, G. Rodrigues, A. Silveira, S. Saleska, Height above the nearest drainage–a hydrologically relevant new terrain model, Journal of Hydrology 404 (1-2) (2011) 13–29.

[22] F. Aristizabal, F. Salas, G. Petrochenkov, T. Grout, B. Avant, B. Bates, R. Spies, N. Chadwick, Z. Wills, J. Judge, Extending height above nearest drainage to model multiple fluvial sources in flood inundation mapping applications for the us national water model, Water Resources Research 59 (5) (2023) e2022WR032039.